JOC The Journal of Organic Chemistry

Article

pubs.acs.org/joc

Synthesis of Crystalline Molecular Gyrotops and Phenylene Rotation inside the Cage

Wataru Setaka,*[,†] Kazuyuki Inoue,[‡] Sayaka Higa,[‡] Seiki Yoshigai,[‡] Hirohiko Kono,[§] and Kentaro Yamaguchi[‡]

[†]Division of Applied Chemistry, Faculty of Urban Environmental Sciences, Tokyo Metropolitan University, Hachioji, Tokyo 192-0397, Japan

[‡]Faculty of Pharmaceutical Sciences at Kagawa Campus, Tokushima Bunri University, Sanuki, Kagawa 769-2193, Japan

[§]Department of Chemistry, Graduate School of Science, Tohoku University, Sendai 980-8578, Japan

Supporting Information

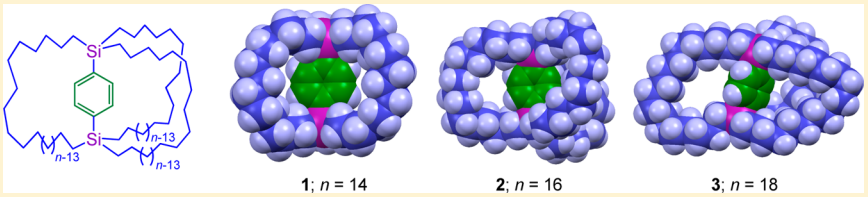

ABSTRACT: Phenylene-bridged macrocage molecules were synthesized as molecular gyrotops because the rotor can rotate even in a crystal. The chain-length-dependent properties of the molecular gyrotops were investigated in order to explore the potential to create new molecular materials. The formation of the cage in the synthesis of each molecular gyrotop depended on the length of the alkyl chains of the precursor. The rotation modes and energy barriers for phenylene rotation inside the crystals of the molecular gyrotops were changed by varying the chain length of the cage.

INTRODUCTION

Molecular rotors, which show rotation of a part of the molecule, have been studied widely. The physical and chemical properties of the molecules tend to be affected by the molecular motion; therefore, the control of molecular motion inside a single crystal has been investigated to explore the potential for the creation of new molecular materials. Thus, much attention has been focused on the chemistry of molecular machines that exhibit mechanical motions of parts of the molecules.[1] Indeed, a number of molecular rotors have been designed, synthesized, and characterized to date, and their rotational dynamics have been revealed.[1−7]

In particular, the chemistry of partial molecular rotations in the crystalline state has been studied. Macrocyclic molecules having a rotor surrounded by a three-spoke stator are expected to have functions of gyroscopes and gyrotops (Figure 1).[2−6] The chemistry of molecular gyroscopes and gyrotops and related molecules has been reported by Garcia-Garibay and co-workers,[2,6] Gladysz and co-workers,[3] and our group.[4,5] The synthesis and dynamics of the rotors have also been studied, and the rotor functions have been reported recently. Studies of the physical properties that change as a result of thermally induced rotation of the rotor are both interesting and important for the development of new functions and applications of organic molecules.

We recently reported the synthesis and properties of crystalline molecular gyrotops having a phenylene rotor surrounded by three long alkyl spokes. Especially, a single crystal of molecular gyrotop **1** (Figure 1) showed temperature-dependent birefringence, which was reported as the first change in optical properties due to the rotation of a phenylene rotor in a crystal.[5d] A similar molecular gyrotop exhibited remarkable inflation of the cage in the crystalline state due to the dynamics of the phenylene rotor, and an unusually high thermal expansion coefficient of the crystal was observed, suggesting a novel function for the dynamic states of the molecules.[5e]

Control of the rotation, for example, its orientation and energy barriers, may allow the creation of novel functional materials based on the dynamic states of the rotor. We recently reported that 1,4-naphthalenediyl-bridged molecular gyrotops

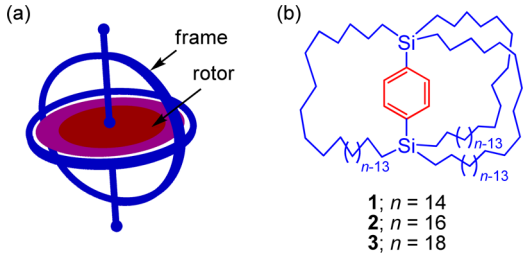

Figure 1. (a) Schematic representation of a gyrotop, which consists of a cage and a rotor. (b) Structural formula of the molecular gyrotops studied.

Received: July 11, 2014
Published: July 25, 2014

   dx.doi.org/10.1021/jo501539h | J. Org. Chem. 2014, 79, 8288−8295

Scheme 1

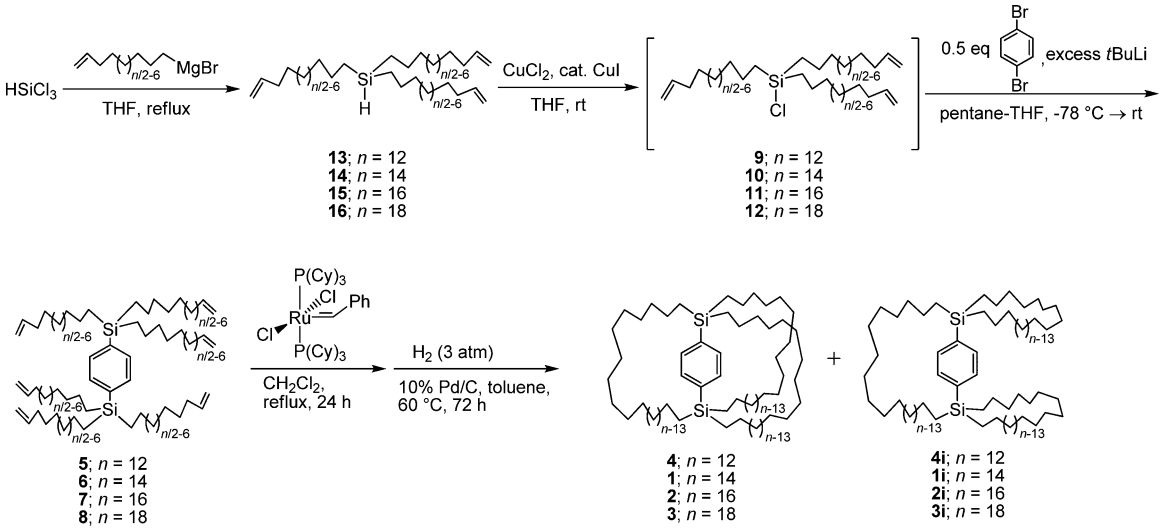

with various cage sizes showed a chain-length dependence of the energy barrier for the rotation of the rotor in solution.[5c] In that study, it was found that the molecular gyrotop surrounded by three tetradecyl (C_{14}) chain derivatives did not show rotation of the naphthalenediyl inside the cage in solution, whereas the 1,4-naphthalenediyl moieties of the gyrotops with hexadecyl (C_{16}) and octadecyl (C_{18}) chain derivatives showed restricted and rapid rotation about an axis in solution, respectively. Therefore, the rotation of the naphthalenediyl rotor in molecular gyrotops can be controlled *in solution* by changing the size of the cage steric effects.

Here we report the chain-length dependence of the formation and rotation mode of the rotor inside the cage *in the crystalline state*. The properties of the molecular gyrotop **1** with C_{14} chains were compared to those of molecular gyrotops with C_{16} chains (**2**) and C_{18} chains (**3**).

RESULTS AND DISCUSSION

Synthesis of the Molecular Gyrotops. Molecular gyrotops and gyroscopes consist of a cage and a rotor (Figure 1). In the present molecular gyrotops, the cage was constructed of three long alkyl spokes, and a benzene ring was applied as a rotor. Benzene is known to have a strong anisotropy in its physical properties in the in-plane and out-of-plane directions because of its planar structure; therefore, its physical properties may be switched to isotropic by rotation of the ring.

The route for the synthesis of the molecular gyrotops is shown in Scheme 1. The syntheses of **1**[5d] and **3**[5a] have been reported previously, whereas the synthesis of **2** was newly achieved by applying the same method, as described in the following. The reaction of trichlorosilane with ω-alkenylmagnesium bromides gave trialkenylsilanes **13**–**16**. After chlorination of the trialkenylsilanes, the reactions of *p*-dilithiobenzene with the resulting trialkenylchlorosilanes afforded *p*-bis(tri-ω-alkenylsilyl)benzenes **5**–**8**. Ring-closing metathesis (RCM)[8] of the bis(silyl)benzenes followed by hydrogenation under 3 atm H_2 in the presence of Pd/C afforded a mixture of the cage and byproducts. The cage compounds were isolated from the reaction mixture by preparative gel-permeation chromatography (GPC). These isolated compounds were identified by ^{1}H and ^{13}C NMR spectroscopy.

The yields of the cage and noncage isomers obtained by RCM of precursors **5**–**8** are summarized in Table 1. We

Table 1. Yields of the Cages and their Noncage Isomers in RCM Reactions of Bis(silyl)benzenes 5–8

	yields/%		
precursor	cage	isomer	isomer/cage ratio[a]
5 (n = 12)	0[c]	0[c]	–
6 (n = 14)[b]	24	0	0
7 (n = 16)	10	43	4.3
8 (n = 18)[d]	23	39	1.7

[a]Formation ratio. [b]Reference 5d. [c]Not detected. [d]Reference 5a.

recently reported the optimization of the reaction conditions of the RCM; we applied the reaction using Grubbs' first-generation catalyst under reflux, which are the best conditions for cage production.[5a] Although the desired cage was not produced by the reaction of bis(silyl)benzene **5**, the highest cage yield was achieved by the RCM of **6**. Hence, the dodecyl (C_{12}) spokes were too short to form the cage, whereas the C_{14} spokes were suitable for the phenylene rotor. In the syntheses of **2** and **3**, noncage isomers **2i** and **3i** were also obtained, probably because the side chains of the cages were too long for the phenylene rotor. The sum of the yields of the cage and noncage isomers was less than 65% in all cases. Thus, the major products of these reactions were polymeric byproducts, although highly dilute conditions were applied in order to prevent intermolecular RCM. Remarkably, the chain length of the precursor affected the formation ratio of the cage and noncage isomers, that is, this ratio plausibly depends on the stability of the reaction intermediates and the products because of the RCM equilibrium reaction.[8] Although the statistical formation ratio of the cage isomer to the noncage isomer is 1:3, as described in the previous report,[5a] the cage is the dominant isomer in the syntheses of **1** and **3**.

The stereochemistry of alkene junctions formed by RCM reactions was investigated before the hydrogenation reaction. Although only the (*E*,*E*,*E*) cage was obtained before hydrogenation in the synthesis of **1**,[5e] a complex mixture including both *E* and *Z* junctions was formed in the syntheses of **2** and **3**,[5a] probably because of the long chains of the cages.

dx.doi.org/10.1021/jo501539h | J. Org. Chem. 2014, 79, 8288–8295

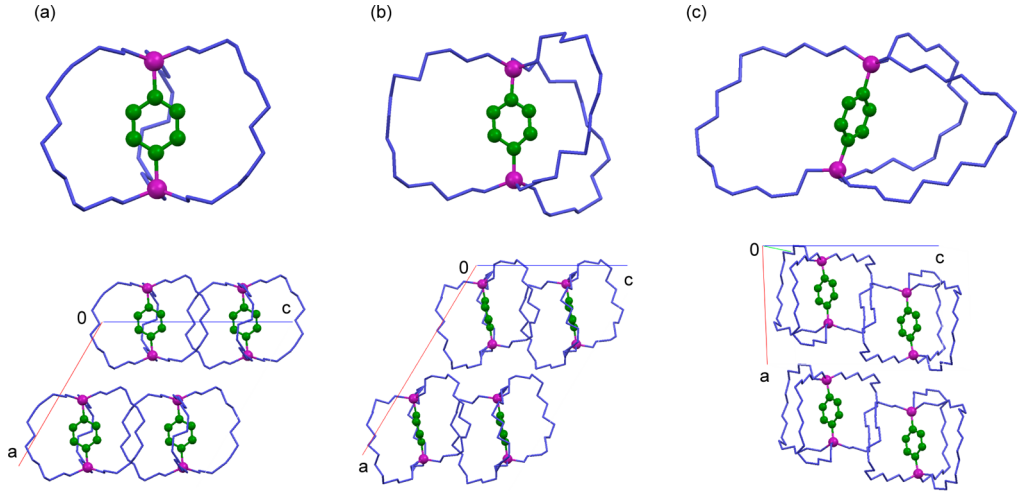

Figure 2. Molecular structures of (a) **1**,[5d] (b) **2**, and (c) **3**[5a] as determined by X-ray crystallography: (top) ball-and-stick models of the molecules; (bottom) packing diagrams. Hydrogen atoms and disordered atoms on the side chains have been omitted for clarity.

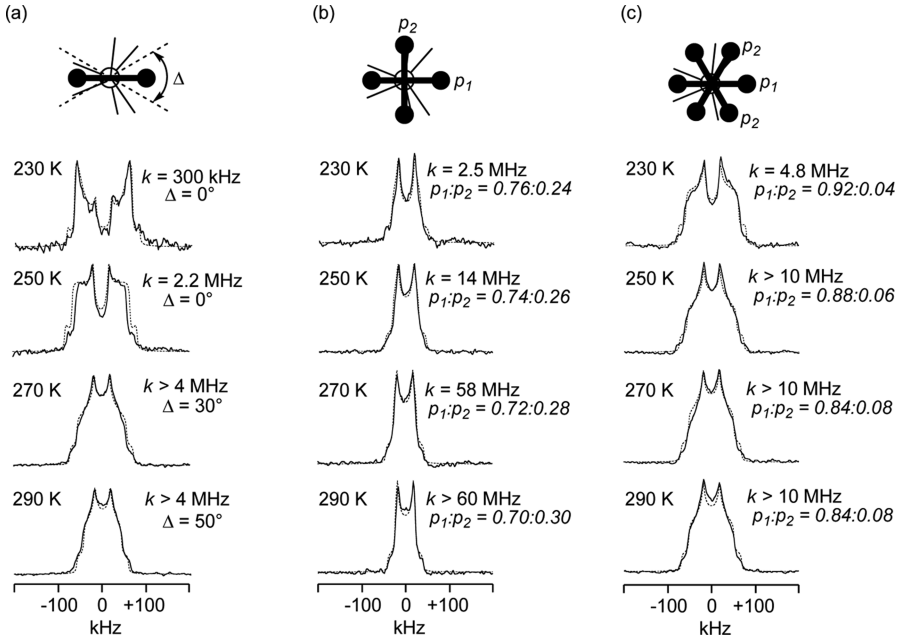

Figure 3. Temperature-dependent solid-state ^{2}H NMR spectra of (a) **1**-d_4 (ref 5d), (b) **2**-d_4, and (c) **3**-d_4 [observed spectra, solid lines; simulated spectra, dotted lines). A schematic drawing of exchange mechanism is shown above each spectrum. Estimated exchange rate constants k, angular displacements Δ, and ratios of populations of the phenylene sites (p_1:p_2) are shown].

X-ray Crystallographic Analyses of the Molecular Gyrotops. The structures of **1** and **3** were determined by X-ray diffraction of single crystals obtained through recrystallization from tetrahydrofuran/methanol solutions, as reported previously.[5a,d] Similarly, recrystallization of the purified molecular gyrotop **2** afforded single crystals suitable for X-ray diffraction. Figure 2 shows the molecular structures of the molecular gyrotops **1**−**3** in the corresponding single crystals as determined by X-ray crystallography. The single crystal of **2** was formed as an overly thin plate and cracked when the temperature was lowered; thus, the X-ray diffraction study of the single crystal of **2** had to be carried out at a relatively high temperature (270 K). In all of the cage compounds, the three alkyl chains effectively surround the phenylene moiety. The crystal structures of **1** and **2** are almost identical, having the same crystal system (monoclinic) and similar space groups ($C2/c$ for **1** and Cc for **2**). Indeed, the shapes of cages of **1** and **2** are almost spherical. Although **1** has C_2 symmetry (with the C_2 axis perpendicular to the rotation axis of the rotor), **2** possesses no symmetry inside the molecule. On the other hand, cage **3**, in which two of the three alkyl chains are separated, is completely different from **1** and **2** because of its different crystal system (triclinic). The results indicate that the alkyl chains of **3** are too long to form a spherical cage.

Packing diagrams of the crystals of **1**−**3** are also shown in Figure 2. In all of the crystals, the molecules are arranged according to their rotation axes. In the crystal structures of **1** with **2**, the phenylenes are arranged perpendicularly about a slightly titled rotation axis.

Phenylene Dynamics of the Molecular Gyrotops in the Crystals. The rates and angular ranges of the phenylene flips inside the crystals were estimated by solid-state ^{2}H NMR

dx.doi.org/10.1021/jo501539h | J. Org. Chem. 2014, 79, 8288−8295

spectroscopy.[9] In a previous report, the temperature-dependent solid-state ^{2}H NMR spectra of **1**-d_4 (in which the phenylene moiety was labeled with four deuterium atoms) were investigated.[5d] The phenylene ring of **1**-d_4 slowly undergoes a 180° flip between the two equilibrium sites that were confirmed by X-ray structural analysis.[5d] The flipping rate was accelerated with increasing temperature between 230 and 260 K. The activation energy (E_a) for the phenylene flip of **1**-d_4 was estimated to be 10.3 kcal/mol from the Arrhenius plot of the flipping rates.[5d] The line widths of the observed spectra narrowed above 270 K, indicating continuous rotation of the phenylene moiety in **1**-d_4 at a rate exceeding the fast-exchange limit (>4 MHz). The spectra were theoretically reproduced by assuming a 180° flip in the fast-exchange limit (4 MHz) with an angular displacement (Δ) that is comparable to the 2σ range of the oscillation angle of the phenylene around the equilibrium position with a Gaussian distribution (cf. Figure 3a).

In contrast to the phenylene flipping with angular displacement observed for **1**-d_4 in the crystal, the phenylene of **2**-d_4 showed different dynamic behavior inside the crystal. Figure 3b displays the temperature-dependent solid-state ^{2}H NMR spectra of **2**-d_4. The line shape of the spectrum at 230 K is different from that of **1**-d_4. The observed spectra were simulated by assuming a 90° jump with unequal populations ($p_1 \neq p_2$).[10] With increasing temperature, the rate of jumping increased, and the populations were averaged in the range 230–290 K.

On the other hand, the phenylene of **3**-d_4 showed another dynamic behavior inside the crystal. Figure 3c displays the temperature-dependent solid-state ^{2}H NMR spectra of **3**-d_4. With increasing temperature, the line widths of the observed spectra narrowed and the shapes of the spectra altered. The observed spectra were theoretically reproduced by assuming a six-site exchange mechanism and applying different populations of benzene rings that can exist at three positions every 120° around the axis of rotation.[10] The simulated spectra reproduced the observed spectra accurately. It is difficult to distinguish precisely between the "six-site exchange applying different populations" mechanism for **3**-d_4 and the "180° flip with angular displacements" mechanism for **1**-d_4 because these mechanisms are intrinsically identical. In this work, if the angular displacements around the equilibrium positions were observed on the NMR time scale, the exchange mechanism is assigned as the "six-site exchange applying different populations" mechanism.

The temperature-dependent ^{2}H NMR spectra of the molecular gyrotops **1**-d_4, **2**-d_4, and **3**-d_4 were completely reversible over the temperature range 220–350 K. The dynamic behaviors of the phenylene rotors in the molecular gyrotops are basically similar, as they show thermally accelerated rotation with angular displacements. However, slightly different mechanisms are needed for the precise analysis of the spectra. These differences in the rotation mechanism may be ascribed to subtle differences in the cage structure that determine the rotational potentials, as described later.

For the estimation of the energy barrier for the rotation of the phenylene, the temperature-dependent spin–lattice relaxation time (T_1) was investigated.[9] The inversion–recovery quadrupole echo pulse sequence was used to measure the T_1 values for the molecular gyrotops. Figure 4 compares the experimentally determined ^{2}H NMR T_1 values for molecular gyrotops **1**-d_4, **2**-d_4, and **3**-d_4 with the calculated T_1 values. The T_1 values are remarkably dependent on temperature and exhibit

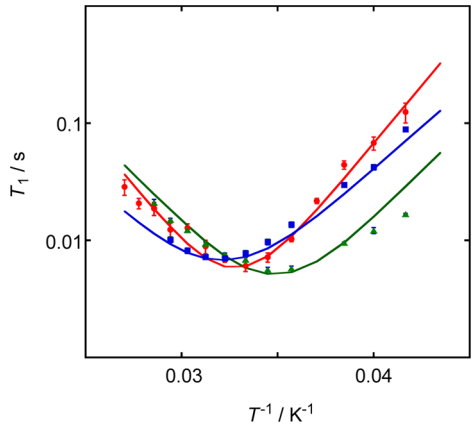

Figure 4. Temperature-dependent ^{2}H spin–lattice relaxation times (T_1) in molecular gyrotops **1** (red circles; ref 5d), **2** (green triangles), and **3** (blue squares) in crystal form. The lines are fits to the relaxation model shown in eq 1, for which the parameters are listed in Table 2.

typical nuclear quadrupolar relaxation with a sharp minimum. The relaxation model shown in eq 1 was used to analyze the temperature dependence of T_1:

$$\frac{1}{T_1} = K\left(\frac{\tau}{1+\omega_0^2\tau^2} + \frac{4\tau}{1+4\omega_0^2\tau^2}\right) \quad (1)$$

where K is an effective coupling constant that depends on the quadruple coupling constant, τ is a single correlation time that obeys the Arrhenius rule [i.e., $\tau = \tau_\infty \exp(E_a/RT)$], and $\omega_0/2\pi$ is the Larmor frequency of deuterium. According to this model, the observed T_1 values were consistent with the calculated ones. The best fit parameters for these calculations using the relaxation model shown in eq 1 are given in Table 2. These

Table 2. Fit Parameters[a] for the Theoretical Curves of T_1 as a Function of Temperature for Gyrotops 1–3

gyrotop	K	τ_∞/s	E_a/kcal mol^{-1}
1 (n = 14)[b]	5.8×10^{10}	4.65×10^{-16} [b]	9.0[b]
2 (n = 16)	6.6×10^{10}	3.0×10^{-15}	7.4
3 (n = 18)	5.0×10^{10}	3.0×10^{-14}	6.6

[a] $\omega_0/2\pi$ = 76.7 MHz. [b] Reference 5d.

results indicate that the phenylene flip was enhanced with increasing temperature and that the rates completely exhibited the Arrhenius behavior over the temperature range 230–370 K (at least). The activation energies were estimated to be 9.0, 7.4, and 6.6 kcal mol^{-1} for **1**-d_4, **2**-d_4, and **3**-d_4, respectively. These values decrease with increasing cage size, indicating that the steric interactions between the phenylene and the cage affect the energy barrier.

DFT Calculations on Molecular Gyrotops. DFT calculations were performed to estimate the energy barriers for phenylene rotation in molecular gyrotops **1**–**3**. First, the molecular structures were optimized at the B3LYP/6-31G* level using the Gaussian 09 program package,[11] and the initial coordinates of the atoms were taken from the single-crystal X-ray analysis data. The optimized structures and X-ray structures were comparable, as shown in Figure 5. For the confirmation of a qualitative agreement between these structures, root-mean-square distances (RMSd) between all silicon and carbon pairs were estimated; these values were 0.451, 1.009, and 0.369 Å for

dx.doi.org/10.1021/jo501539h | J. Org. Chem. 2014, 79, 8288–8295

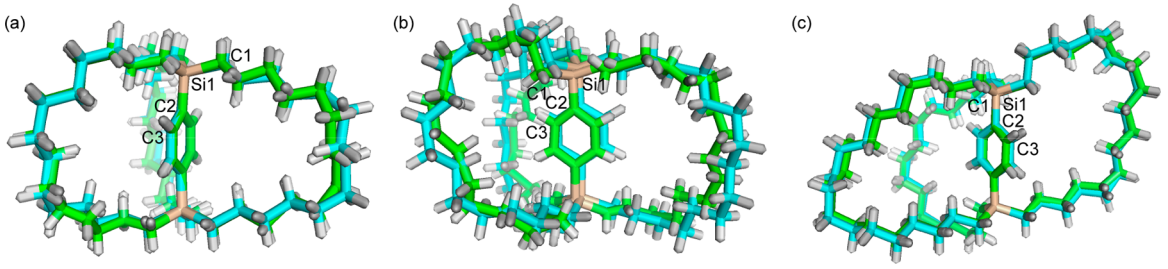

Figure 5. Comparison between the X-ray structures (green) and optimized structures from DFT calculations (B3LYP/6-31G*) (sky blue). RMS distances (RMSd) between all silicon and carbon pairs and C1−Si1−C2−C3 dihedral angles θ determined by X-ray crystallography and DFT calculations: (a) **1** [RMSd = 0.451 Å for 50 pairs; θ = 101.0° (X-ray), 104.90 (calcd)]; (b) **2** [RMSd = 1.009 Å for 56 pairs; θ = 54.9° (X-ray), 40.58° (calcd)]; (c) **3** [RMSd = 0.369 Å for 62 pairs; θ = −69.3° (X-ray), −88.90° (calcd)].

1, **2**, and **3**, respectively. The small RMSd values indicate that the optimized molecular structures adequately reflect the structures of the molecules in the crystalline state.

The rotational potentials of the phenylene rings in molecular gyrotops **1**, **2**, and **3** were calculated at the B3LYP/6-31G* level. In these calculations, the coordinates of the cages and the two ipso carbons were fixed to those in the optimized structure as shown in Figure 5, and the coordinates of the residual four phenylene CH atoms were optimized at various C1−Si1−C2−C3 dihedral angles θ (see Figure 5). Figure 6 shows the plots of

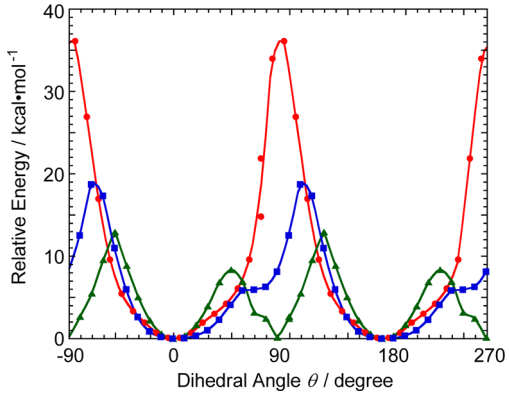

Figure 6. Potential energy for phenylene rotation as a function of the C1−Si−C2−C3 dihedral angle θ (atom labeling shown in Figure 5) calculated at the B3LYP/6-31G* level for **1** (red circles), **2** (green triangles), and **3** (blue squares).

the calculated energy for each dihedral angle, and the dihedral angle of the calculated most stable structure was set equal to 0°. Only one minimum of the potential curve in the θ range between −90° and +90° was observed for **1** and **3**, indicating that a 180° flip between the two equilibrium sites is a plausible mechanism for the phenylene motion. These almost flat potential curves suggest the occurrence of angular displacements of the phenylene at higher temperatures. On the other hand, the potential curve for **2** shows two minima in the range, indicating that a 90° jump mechanism is suitable to describe the phenylene dynamics. These calculated features are in good qualitative agreement with the observed dynamics of the phenylene in these molecules. However, the calculated energy barriers for the phenylene dynamics are higher than the experimentally determined values because relaxation of the cage was not allowed in these calculations. Hence, further investigation is necessary for quantitative analysis of the potential curves.[4b]

CONCLUSION

The chain-length dependence of the properties of molecular gyrotops was investigated. The formation of the cage in the synthesis of the molecular gyrotops depended on the length of the alkyl chains of the precursor. The rotation modes and energy barriers for phenylene rotation inside the crystals of the molecular gyrotops were varied by changing the chain length of the cage. Theoretical calculations of the phenylene rotational potential curves were in good qualitative agreement with the observed dynamics. It is therefore concluded that the potential curves for phenylene rotation in the crystalline state are determined by the structure of the cage in the molecular gyrotop.

EXPERIMENTAL SECTION

General. The reactions were performed under anhydrous conditions using argon, unless otherwise noted. The chemical shifts of ^{1}H (400 MHz) and ^{13}C (100 MHz) NMR spectra are based on the residual solvent resonances. ^{29}Si (79 MHz) NMR chemical shifts are referenced to external tetramethylsilane. The assignment of the NMR signals was carried out by using 1D and 2D NMR techniques (^{1}H, ^{13}C, DEPT, COSY, and HSQC).

Materials. Commercially available reagents were used as received without further purification. Anhydrous THF, hexane, and dichloromethane were purchased from a chemical supplier. Grubbs' catalysts (first and second generation), which are commercially available, were used for the RCM reactions. The syntheses of silanes **14**[5d] and **16**,[5a] bis(silyl)benzenes **6**[5d] and **8**,[5a] and molecular gyrotops **1**,[5d] **3**,[5a] and **3i**[5a] have been reported previously.

Synthesis of Tri-6-heptenylsilane (13). A 1.0 M THF solution of 6-heptenylmagnesium bromide (200 mL, 200 mmol) prepared from the corresponding alkenyl bromide and magnesium was placed into a two-neck flame-dried round-bottom flask (200 mL) equipped with a magnetic stirrer, a condenser, and a dropping funnel. Trichlorosilane (8.13 g, 60 mmol) was introduced dropwise into the reaction flask cooled by a water bath. The reaction mixture was stirred at ambient temperature for 15 h. The mixture was hydrolyzed with dilute HCl(aq) and extracted with hexane. The organic layer was washed with saturated $NaHCO_3$(aq) and dried over anhydrous Na_2SO_4. Concentration and column chromatography [Merck silica gel 60, particle size 63−200 μm, hexane as eluent (R_f = 0.9)] of the residue afforded **13** as a colorless oil (18.35 g, 57.3 mmol, 95% yield). ^{1}H NMR ($CDCl_3$, 400 MHz): δ 0.55−0.62 (m, 6H, SiCH_2), 1.27−1.45 (m, 24H), 2.039 (tddd, J = 7.0, 7.0, 1.7, 1.4 Hz, 6H, H_2C=CH−CH_2−), 3.689 (septet, J = 3.2 Hz, 1H, SiH), 4.926 (ddt, J = 6.8, 2.4, 1.4 Hz, 6H, terminal H_2C=), 4.989 (ddt, J = 16.8, 2.4, 1.5 Hz, 6H, terminal H_2C=), 5.804 (ddt, J = 16.8, 10.4, 6.8 Hz, 6H, H_2C=CH−). ^{13}C NMR ($CDCl_3$, 100 MHz): δ 11.26, 24.53, 28.61, 32.82, 33.72, 114.12 (−CH=CH_2), 139.08 (−CH=CH_2). ^{29}Si NMR ($CDCl_3$, 79.5 MHz): δ −6.49. Anal. Calcd for $C_{21}H_{40}Si$: C, 78.67; H, 12.57. Found: C, 78.63; H, 12.42.

dx.doi.org/10.1021/jo501539h | J. Org. Chem. 2014, 79, 8288−8295

Synthesis of Tri-8-nonenylsilane (15). Compound **15** was synthesized from 8-nonenylmagnesium bromide using the same procedure as for **13** and was obtained as colorless oil in 98% yield. ^{1}H NMR ($CDCl_3$, 400 MHz): δ 0.53−0.62 (m, 6H, SiCH_2), 1.24−1.42 (m, 30H), 2.034 (tddd, J = 7.0, 7.0, 1.7, 1.4 Hz, 6H, H_2C═CH−CH_2−), 3.668 (septet, J = 3.2 Hz, 1H, SiH), 4.918 (ddt, J = 6.8, 2.4, 1.4 Hz, 6H, terminal H_2C═), 4.982 (ddt, J = 16.8, 2.4, 1.5 Hz, 6H, terminal H_2C═), 5.802 (ddt, J = 16.8, 10.4, 6.8 Hz, 6H, H_2C═CH−). ^{13}C NMR ($CDCl_3$, 100 MHz): δ 11.31, 24.67, 28.97, 29.06, 29.17, 33.30, 33.81, 114.08 (−CH═CH_2), 139.16 (−CH═CH_2). ^{29}Si NMR ($CDCl_3$, 79.5 MHz): δ −6.44. Anal. Calcd for $C_{27}H_{52}Si$: C, 80.11; H, 12.95. Found: C, 80.00; H, 13.32.

Synthesis of 1,4-Bis(tri-6-heptenylsilyl)benzene (5). *a. Preparation of the Chlorosilane.* $CuCl_2$ (11.02 g, 82 mmol) and CuI (0.06 g, 0.3 mmol) were placed into a two-neck round-bottom flask (300 mL) equipped with a magnetic stirrer, a condenser, and a dropping funnel. Dry THF (150 mL) was added into the flask. After dropwise addition of **13** (12.8 g, 40 mmol) into the reaction flask, the mixture was stirred at rt for 12 h. The volatile materials were removed under reduced pressure. Anhydrous hexane (∼50 mL) was added to the residual mixture, and cuprous halide was filtered off using Celite. Evaporation of the filtrate afforded **9** (13.36 g, 94% yield) in 80% purity as determined by ^{1}H NMR spectroscopy, and the corresponding siloxane was obtained as a hydrolyzed product. Further purification was not carried out because of the compound's high boiling point and hydrolyzability.

b. Synthesis of the Bis(silyl)benzene. *p*-Dibromobenzene (2.1 g, 9.0 mmol) and dry THF (20 mL) were placed in a Schlenk flask (100 mL). A *tert*-BuLi solution (1.6 M in pentane, 22 mL, 4.0 equiv) was added dropwise to the solution at −78 °C. The reaction mixture turned yellow and was stirred for an additional 1 h at −78 °C. The reaction mixture was warmed to 0 °C, and then chlorosilane **9** (6.5 g, 18.3 mmol) was added. After 12 h of stirring at rt, the mixture was hydrolyzed with dilute HCl(aq) and extracted with hexane. The organic layer was washed with saturated $NaHCO_3$(aq) and dried over anhydrous Na_2SO_4. Concentration and column chromatography [Merck silica gel 60, particle size 63−200 μm, hexane as eluent (R_f = 0.5)] of the residue afforded **5** as a colorless oil (4.4 g, 6.2 mmol, 69% yield). ^{1}H NMR ($CDCl_3$, 400 MHz): δ 0.74−0.81 (m, 12H, SiCH_2), 1.28−1.42 (m, 36H), 2.016 (tddd, J = 7.0, 6.8, 1.7, 1.4 Hz, 12H, H_2C═CH−CH_2−), 4.926 (ddt, J = 10.4, 2.4, 1.4 Hz, 6H, terminal H_2C═), 4.989 (ddt, J = 16.8, 2.4, 1.7 Hz, 6H, terminal H_2C═), 5.804 (ddt, J = 16.8, 10.4, 6.8 Hz, 6H, H_2C═CH−), 7.431 (s, 4H, C_6H_4). ^{13}C NMR ($CDCl_3$, 100 MHz): δ 12.39, 23.65, 28.51, 33.25, 33.74, 114.11 (−CH═CH_2), 133.23 (aromatic CH), 138.31 (SiC), 139.16 (−CH═CH_2). ^{29}Si NMR ($CDCl_3$, 79.5 MHz): δ −2.33. Anal. Calcd for $C_{48}H_{82}Si_2$: C, 80.59; H, 11.55. Found: C, 80.36; H, 11.30.

Synthesis of 1,4-Bis(tri-8-nonenylsilyl)benzene (7). Compound **7** was synthesized from **15** using the same procedure as for **5**. Pure compound **7** (4.4 g, 0.5 mmol, 55% yield) was obtained as a colorless oil. ^{1}H NMR ($CDCl_3$, 500 MHz): δ 0.750 (t, J = 7.5 Hz, 12H, SiCH_2), 1.20−1.40 (m, 48H), 2.019 (tddd, J = 7.0, 6.8, 1.7, 1.4 Hz, 12H, H_2C═CH−CH_2−), 4.914 (ddt, J = 10.4, 2.4, 1.4 Hz, 6H, terminal H_2C═), 4.976 (ddt, J = 16.8, 2.4, 1.7 Hz, 6H, terminal H_2C═), 5.794 (ddt, J = 16.8, 10.4, 6.8 Hz, 6H, H_2C═CH−), 7.412 (s, 4H, C_6H_4). ^{13}C NMR ($CDCl_3$, 125.8 MHz): δ 12.48, 23.82, 28.98, 29.09 (overlapped), 33.76, 33.83, 114.10 (−CH═CH_2), 133.23 (aromatic CH), 138.44 (SiC), 139.23 (−CH═CH_2). ^{29}Si NMR ($CDCl_3$, 99 MHz): δ −2.39. Anal. Calcd for $C_{60}H_{106}Si_2$: C, 81.55; H, 12.09. Found: C, 81.75; H, 12.22.

Synthesis of Molecular Gyrotop 2. A dichloromethane solution (200 mL) of **7** (0.800 g, 0.9 mmol) was added dropwise with stirring over 12 h at 40 °C to a solution of dichloromethane (600 mL) in the presence of Grubbs' first-generation catalyst (0.02 g, 0.02 mmol). During the reaction, the catalyst (0.02 g, 0.06 mmol) was added to the flask twice (every 2 h). The mixture was stirred for a further 8 h. The volatile materials were removed in vacuo, and the benzene-soluble fraction was treated by flash column chromatography (silica gel, benzene) to remove the metal catalysts. The fraction contained unsaturated cyclized mixtures with (*E*/*Z*)-alkenyl junctions (0.8 g). Then hydrogen gas (3 atm) was introduced into a toluene (5 mL) solution of the reaction mixture in the presence of 10% Pd/C (0.03 g) in an autoclave, and the mixture was allowed to stand for 72 h at 60 °C. After the excess H_2 gas was released, the mixture was filtered to remove Pd/C. The volatile materials were removed in vacuo. Fractions containing **2** and **2i** were collected using GPC with chloroform as the solvent. Pure compounds **2** (0.080 g, 0.09 mmol, 10% yield) and **2i** (0.351 g, 0.40 mmol, 43% yield) were obtained after removal of the solvent in vacuo. Compound **2**: colorless crystals, mp 143.3−143.9 °C. ^{1}H NMR ($CDCl_3$, 400 MHz): δ 0.71−0.78 (m, 12H, SiCH_2), 1.18−1.40 (m, 84H), 7.47 (s, 4H, aromatic CH). ^{13}C NMR ($CDCl_3$, 100 MHz): δ 12.42, 23.23, 27.69, 28.12, 28.22, 28.79, 28.89, 32.89, 133.43 (aromatic CH), 138.02 (SiC). ^{29}Si NMR ($CDCl_3$, 79.5 MHz): δ −2.14. Anal. Calcd for $C_{54}H_{100}Si_2$: C, 80.51; H, 12.51. Found: C, 80.40; H, 12.51. Compound **2i**: colorless oil, bp >300 °C. ^{1}H NMR ($CDCl_3$, 400 MHz): δ 0.65−0.72 (m, 4H, SiCH_2), 0.73−0.90 (m, 8H, SiCH_2), 1.15−1.25 (m, 28H), 1.25−1.42 (m, 56H), 7.43 (s, 4H, aromatic CH). ^{13}C NMR ($CDCl_3$, 100 MHz): δ 11.89 (4C), 13.19 (2C), 23.05 (4C), 23.63 (2C), 27.10 (4C), 27.61 (4C), 27.64 (2 × 4C), 27.72 (2C), 27.98 (4C), 28.26 (2C), 28.31 (2C), 28.37 (2C), 28.57 (2C), 32.59 (4C), 33.40 (2C), 133.22 (aromatic CH), 138.40 (SiC). ^{29}Si NMR ($CDCl_3$, 79.5 MHz): δ −1.93. Anal. Calcd for $C_{54}H_{100}Si_2$: C, 80.51; H, 12.51. Found: C, 80.56; H, 12.85.

RCM of Compound 5 for Synthesis of Molecular Gyrotop 4. The RCM reaction of bis(silyl)benzene **5** and subsequent hydrogenation was investigated using the same procedure as for the synthesis of **2**. However, only polymeric products were obtained, and the desired molecular gyrotop **4** and its isomer **4i** were not formed at all.

X-ray Crystallographic Analysis of Molecular Gyrotop 2. The diffraction data of molecular gyrotop **2** were collected using graphite-monochromatized Mo Kα radiation (λ = 0.71069 Å). Crystallographic data for **2** (270 K): monoclinic, *Cc*, a = 28.51(6) Å, b = 12.34(2) Å, c = 17.98(4) Å, β = 121.13(2)°, V = 5414(18) Å^3, R_1 = 0.12.16 [$I > 2\sigma(I)$], wR_2 = 0.4879 (all data). The crystallographic data were deposited at the Cambridge Crystallographic Data Centre (CCDC-1003587). The X-ray crystallographic analyses of **1**, **3** and **3i** were reported previously,[5a,d] and the data were deposited in the CCDC as follows: CCDC-830990 for **1**, CCDC-988815 for **3**, and CCDC-988816 for **3i**.

Solid-State ^{2}H NMR Analysis of Molecular Gyrotops 2-d_4 and 3-d_4. The temperature-dependent solid-state ^{2}H NMR spectra of **2**-d_4 and **3**-d_4 were investigated using the same procedure as reported previously for **1**-d_4.[5d] The details are as follows. The data were recorded using a quadrupolar echo pulse sequence (d_1−90° pulse−τ_1−90° pulse−τ_2−FID; 90° pulse = 4.2 μs, τ_1 = 30 μs, τ_2 = 20 μs, d_1 = 20 s). Simulations of the ^{2}H NMR spectra were performed using NMR-WEBLAB.[10a] The following parameters were used for the simulations: quadrupolar coupling constant (q_{cc}) = 130 kHz, asymmetry parameter (η) = 0, line broadening = 3 kHz. The temperature dependence of the spin−lattice relaxation time (T_1) in the ^{2}H NMR spectra was recorded using an inversion−recovery quadrupolar echo pulse sequence (d_1−180° pulse−d_2−90° pulse−τ_1−90° pulse−τ_2−FID; 90° pulse = 4.2 μs, τ_1 = 30 μs, τ_2 = 20 μs, d_1 = 5−3 s, d_2 varied) and standard T_1 analysis software. The spin−lattice relaxation rate is known to depend on the motional model for the exchange process. Several special types of motions have been discussed to date.[12] Further detailed investigations are required for the determination of parameters for the appropriate special model.

DFT Calculations for Molecular Gyrotops. The molecular structures were optimized using Gaussian 09, revision D.01, and the initial coordinates of atoms were taken from the single-crystal X-ray analysis data. The structural parameters of the optimized structures are shown in the Supporting Information. In the calculations of the rotational potentials of the phenylene ring in molecular gyrotops **1**−**3**, the coordinates of the cages and two ipso carbons were fixed to those in the optimized structure, and the coordinates of the residual four phenylene CH atoms were optimized at various dihedral angles θ.

dx.doi.org/10.1021/jo501539h | J. Org. Chem. 2014, 79, 8288−8295

■ ASSOCIATED CONTENT

Supporting Information

Copies of NMR spectra for all new compounds (**2**, **2i**, **5**, **7**, **13**, and **15**), details of the solid-state ^{2}H NMR study of **2**-d_4 and **3**-d_4, atomic coordinates from DFT calculations on **1**−**3**, and a CIF file for compound **2**. This material is available free of charge via the Internet at http://pubs.acs.org.

■ AUTHOR INFORMATION

Corresponding Author

*E-mail: wsetaka@tmu.ac.jp.

Notes

The authors declare no competing financial interest.

■ ACKNOWLEDGMENTS

This work was supported by a JSPS Grant-in-Aid for Scientific Research (B) (25288042) and the Kurata Memorial Hitachi Science and Technology Foundation.

■ REFERENCES

(1) (a) Vogelsberg, C. S.; Garcia-Garibay, M. A. *Chem. Soc. Rev.* **2012**, *41*, 1892. (b) Karim, A. R.; Linden, A.; Baldridge, K. K.; Siegel, J. S. *Chem. Sci.* **2010**, *1*, 102. (c) Balzani, V.; Credi, A.; Venturi, M. *Molecular Devices and Machines*, 2nd ed.; Wiley-VCH: Weinheim, Germany, 2008. (d) Leigh, D. A.; Zerbetto, F.; Kay, E. R. *Angew. Chem., Int. Ed.* **2007**, *46*, 72. (e) Browne, W. R.; Feringa, B. L. *Nat. Nanotechnol.* **2006**, *1*, 25. (f) Kelly, T. R. *Molecular Machines*; Topics in Current Chemistry, Vol. *262*; Springer: Berlin, 2005. (g) Kottas, G. S.; Clarke, L. I.; Horinek, D.; Michl, J. *Chem. Rev.* **2005**, *105*, 1281. (h) Garcia-Garibay, M. A. *Proc. Natl. Acad. Sci. U.S.A.* **2005**, *102*, 10771. (i) Balzani, V.; Credi, A.; Raymo, R.; Stoddart, J. F. *Angew. Chem., Int. Ed.* **2000**, *39*, 3348.

(2) (a) Commins, P.; Garcia-Garibay, M. A. *J. Org. Chem.* **2014**, *79*, 1611. (b) Commins, P.; Nuñez, J. E.; Garcia-Garibay, M. A. *J. Org. Chem.* **2011**, *76*, 8355. (c) Nuñez, J. E.; Natarajan, A.; Khan, S. I.; Garcia-Garibay, M. A. *Org. Lett.* **2007**, *9*, 3559.

(3) (a) Nawara-Hultzsch, A. J.; Stollenz, M.; Barbasiewicz, M.; Szafert, S.; Lis, T.; Hampel, F.; Bhuvanesh, N.; Gladysz, J. A. *Chem.—Eur. J.* **2014**, *20*, 4617. (b) Zeits, P. D.; Rachiero, G. P.; Hampel, F.; Reibenspies, J. H.; Gladysz, J. A. *Organometallics* **2012**, *31*, 2854. (c) Skopek, K.; Gladysz, J. A. *J. Organomet. Chem.* **2008**, *693*, 857. (d) Skopek, K.; Barbasiewicz, M.; Hampel, F.; Gladysz, J. A. *Inorg. Chem.* **2008**, *47*, 3474. (e) Han, J.; Deng, C.; Wang, L.; Gladysz, J. A. *Organometallics* **2010**, *29*, 3231. (f) Heß, G. D.; Hampel, F.; Gladysz, J. A. *Organometallics* **2007**, *26*, 5129. (g) Wang, L.; Shima, T.; Hampel, F.; Gladysz, J. A. *Chem. Commun.* **2006**, 4075. (h) Wang, L.; Hampel, F.; Gladysz, J. A. *Angew. Chem., Int. Ed.* **2006**, *45*, 4372. (i) Narwara, A. J.; Shima, T.; Hampel, F.; Gladysz, J. A. *J. Am. Chem. Soc.* **2006**, *128*, 4962. (j) Shima, T.; Hampel, F.; Gladysz, J. A. *Angew. Chem., Int. Ed.* **2004**, *43*, 5537.

(4) (a) Setaka, W.; Ohmizu, S.; Kira, M. *Chem. Commun.* **2014**, *50*, 1098. (b) Marahatta, A. B.; Kanno, M.; Hoki, K.; Setaka, W.; Irle, S.; Kono, H. *J. Phys. Chem. C* **2012**, *116*, 24845. (c) Setaka, W.; Ohmizu, S.; Kira, M. *Chem. Lett.* **2010**, *39*, 468. (d) Setaka, W.; Ohmizu, S.; Kabuto, C.; Kira, M. *Chem. Lett.* **2007**, *36*, 1076.

(5) (a) Setaka, W.; Higa, S.; Yamaguchi, K. *Org. Biomol. Chem.* **2014**, *12*, 3354. (b) Setaka, W.; Yamaguchi, K. *J. Am. Chem. Soc.* **2013**, *135*, 14560. (c) Setaka, W.; Koyama, A.; Yamaguchi, K. *Org. Lett.* **2013**, *15*, 5092. (d) Setaka, W.; Yamaguchi, K. *Proc. Natl. Acad. Sci. U.S.A.* **2012**, *109*, 9260. (e) Setaka, W.; Yamaguchi, K. *J. Am. Chem. Soc.* **2012**, *134*, 12458. (f) Setaka, W.; Yamaguchi, K. Patent JP5235927, April 5, 2013. (g) Setaka, W.; Yamaguchi, K. Patent JP5274506, May 24, 2013.

(6) (a) Dominguez, Z.; Dang, H.; Strouse, M. J.; Garcia-Garibay, M. A. *J. Am. Chem. Soc.* **2002**, *124*, 2398. (b) Godinez, C. E.; Zepeda, G.; Garcia-Garibay, M. A. *J. Am. Chem. Soc.* **2002**, *124*, 4701. (c) Dominguez, Z.; Dang, H.; Strouse, J. M.; Garcia-Garibay, M. A. *J. Am. Chem. Soc.* **2002**, *124*, 7719. (d) Dominguez, Z.; Khuong, T. A. V.; Sanrame, C. N.; Dang, H.; Nuñez, J. E.; Garcia-Garibay, M. A. *J. Am. Chem. Soc.* **2003**, *125*, 8827. (e) Horansky, R. D.; Clarke, L. I.; Winston, E. B.; Price, J. C.; Karlen, S. D.; Jarowski, P. D.; Santillan, R.; Garcia-Garibay, M. A. *Phys. Rev. B* **2006**, *74*, No. 054306. (f) Horansky, R. D.; Clarke, L. I.; Price, J. C.; Khuong, T.-A. V.; Jarowski, P. D.; Garcia-Garibay, M. A. *Phys. Rev. B* **2005**, *72*, No. 014302. (g) Vogelsberg, C. S.; Bracco, S.; Beretta, M.; Comotti, A.; Sozzani, P.; Garcia-Garibay, M. A. *J. Phys. Chem. B* **2012**, *116*, 1623. (h) Czajkowska-Szczykowska, D.; Rodríguez-Molina, B.; Magaña-Vergara, N. E.; Santillan, R.; Morzycki, J. W.; Garcia-Garibay, M. A. *J. Org. Chem.* **2012**, *77*, 9970. (i) Rodríguez-Molina, B.; Pérez-Estrada, S.; Garcia-Garibay, M. A. *J. Am. Chem. Soc.* **2013**, *135*, 10388. (j) Rodríguez-Molina, B.; Ochoa, M. E.; Romero, M.; Khan, S. I.; Farfán, N.; Santillan, R.; Garcia-Garibay, M. A. *Cryst. Growth Des.* **2013**, *13*, 5107. (k) Torres-Huerta, A.; Rodríguez-Molina, B.; Höpfl, H.; Garcia-Garibay, M. A. *Organometallics* **2014**, *33*, 354. (l) Jiang, X.; Rodríguez-Molina, B.; Nazarian, N.; Garcia-Garibay, M. A. *J. Am. Chem. Soc.* **2014**, *136*, 8871−8874.

(7) (a) Bastien, G.; Lemouchi, C.; Wzietek, P.; Simonov, S.; Zorina, L.; Rodríguez-Fortea, A.; Canadell, E.; Batail, P. *Z. Anorg. Allg. Chem.* **2014**, *640*, 1127. (b) Lemouchi, C.; Yamamoto, H.; Kato, R.; Simonov, S.; Zorina, L.; Fortea, A. R.; Canadell, E.; Wzietek, P.; Iliopoulos, K.; Gindre, D.; Chrysos, M.; Batail, P. *Cryst. Growth Des.* **2014**, *14*, 3375. (c) Comotti, A.; Bracco, S.; Yamamoto, A.; Beretta, M.; Hirukawa, T.; Tohnai, N.; Miyata, M.; Sozzani, P. *J. Am. Chem. Soc.* **2014**, *136*, 618. (d) Lemouchi, C.; Iliopoulos, K.; Zorina, L.; Simonov, S.; Wzietek, P.; Cauchy, T.; Rodríguez-Fortea, A.; Canadell, E.; Kaleta, J.; Michl, J.; Gindre, D.; Chrysos, M.; Batail, P. *J. Am. Chem. Soc.* **2013**, *135*, 9366. (e) Sugino, H.; Kawai, H.; Fujiwara, K.; Suzuki, T. *Chem. Lett.* **2012**, *41*, 79. (f) Shustova, N. B.; Ong, T.-C.; Cozzolino, A. F.; Michaelis, V. K.; Griffin, R. G.; Dincă, M. *J. Am. Chem. Soc.* **2012**, *134*, 15061. (g) Khan, N. S.; Perez-Aguilar, J. M.; Kaufmann, T.; Hill, P. A.; Taratula, O.; Lee, O.-S.; Carroll, P. J.; Saven, J. G.; Dmochowski, I. J. *J. Org. Chem.* **2011**, *76*, 1418. (h) Comotti, A.; Bracco, S.; Valsesia, P.; Beretta, M.; Sozzani, P. *Angew. Chem., Int. Ed.* **2010**, *49*, 1760. (i) Kitagawa, H.; Kobori, Y.; Yamanaka, M.; Yoza, K.; Kobayashi, K. *Proc. Natl. Acad. Sci. U.S.A.* **2009**, *106*, 10444. (j) Brustolon, M.; Barbon, A.; Bortolus, M.; Maniero, A. L.; Sozzani, P.; Comotti, A.; Simonutti, R. *J. Am. Chem. Soc.* **2004**, *126*, 15512.

(8) (a) Herndon, J. W. *Coord. Chem. Rev.* **2014**, *272*, 48. (b) Fürstner, A. *Science* **2013**, *341*, 1229713. (c) *Handbook of Metathesis*; Grubbs, R. H., Ed.; Wiley-VCH: Weinheim, Germany, 2003; Vols. *1*−*3*. (d) Schrock, R. R. *Angew. Chem., Int. Ed.* **2006**, *45*, 3748. (e) Grubbs, R. H. *Angew. Chem., Int. Ed.* **2006**, *45*, 3760. (f) Vougioukalakis, G. C.; Grubbs, R. H. *Chem. Rev.* **2010**, *110*, 1746.

(9) (a) Hoatson, G. L.; Vold, R. L. *NMR: Basic Princ. Prog.* **1994**, *32*, 1. (b) Spiess, H. W. *Colloid Polym. Sci.* **1983**, *261*, 193. (c) Simpson, J. H.; Rice, D. M.; Karasz, F. E. *J. Polym. Sci., Part B: Polym. Phys.* **1992**, *30*, 11. (d) Cholli, A. L.; Dumais, J. J.; Engel, A. K.; Jelinski, L. W. *Macromolecules* **1984**, *17*, 2399.

(10) (a) Macho, V.; Brombacher, L.; Spiess, H. W. *Appl. Magn. Reson.* **2001**, *20*, 405−432. (b) Hansen, M. R.; Graf, R.; Spiess, H. W. *Acc. Chem. Res.* **2013**, *46*, 1996. (c) Schmidt-Rohr, K.; Spiess, H. W. *Multidimensional Solid-State NMR and Polymers*; Academic Press: London, 1994.

(11) All calculations were performed using Gaussian 09: Frisch, M. J.; Trucks, G. W.; Schlegel, H. B.; Scuseria, G. E.; Robb, M. A.; Cheeseman, J. R.; Scalmani, G.; Barone, V.; Mennucci, B.; Petersson, G. A.; Nakatsuji, H.; Caricato, M.; Li, X.; Hratchian, H. P.; Izmaylov, A. F.; Bloino, J.; Zheng, G.; Sonnenberg, J. L.; Hada, M.; Ehara, M.; Toyota, K.; Fukuda, R.; Hasegawa, J.; Ishida, M.; Nakajima, T.; Honda, Y.; Kitao, O.; Nakai, H.; Vreven, T.; Montgomery, J. A., Jr.; Peralta, J. E.; Ogliaro, F.; Bearpark, M.; Heyd, J. J.; Brothers, E.; Kudin, K. N.; Staroverov, V. N.; Kobayashi, R.; Normand, J.; Raghavachari, K.; Rendell, A.; Burant, J. C.; Iyengar, S. S.; Tomasi, J.; Cossi, M.; Rega, N.; Millam, J. M.; Klene, M.; Knox, J. E.; Cross, J. B.; Bakken, V.; Adamo, C.; Jaramillo, J.; Gomperts, R.; Stratmann, R. E.; Yazyev, O.; Austin, A. J.; Cammi, R.; Pomelli, C.; Ochterski, J. W.; Martin, R. L.;

Morokuma, K.; Zakrzewski, V. G.; Voth, G. A.; Salvador, P.; Dannenberg, J. J.; Dapprich, S.; Daniels, A. D.; Farkas, Ö.; Foresman, J. B.; Ortiz, J. V.; Cioslowski, J.; Fox, D. J. *Gaussian 09*, revision D.01; Gaussian, Inc.: Wallingford, CT, 2013.

(12) Spiess, H. W. *NMR Basic Principles and Progress*; Diehl, P.; Fluck, E.; Kosfeld, R., Eds.; Springer: Berlin, 1978.